ISSN: 2538-2152; ECOPERSIA 2022; 10(1):71-83.

Application of pixel-based and object-based approaches for LULC mapping in Jiroft region, S.E. Iran

ARTICLEINFO

Article Type
Original Research

Authors
Asghar Eslami, *.M.Sc.*[1]
Sedigheh Anvari, *Ph.D.*[2*]
Neamat Karimi, *Ph.D.*[3]
Sedigheh Mohammadi, *Ph.D.*[4]

How to cite this article
Eslami A., Anvari S., Karimi N., Mohammadi S. Application of pixel-based and object-based approaches for LULC mapping in Jiroft region, S.E. Iran. ECOPERSIA 2022; 10(1): 71-83.

DOR:
20.1001.1.23222700.2022.10.1.7.0

[1] M.Sc, Department of Water Resources Management, Faculty of Civil Engineering and Geodesy, Graduate University of Advanced Technology, Kerman, Iran
[2] Ph.D, Department of Ecology, Institute of Science and High Technology and Environmental Science, Graduate University of Advanced Technology, Kerman, Iran.
[3] Ph.D, Department of Water Resources Study and Research, Water Research Institute, Tehran, Iran.
[4] Ph.D, Department of Ecology, Institute of Science and High Technology and Environmental Science, Graduate University of Advanced Technology, Kerman, Iran

**** Correspondence***
Address: Graduate University of Advanced Technology, Kerman, Iran.
Postal Code: 7631133131
Phone: +98 (34) 33776611
Fax: +98 (34) 33776617
Email: anvari.t@gmail.com

Article History
Received: September 3, 2021
Accepted: November 6, 2021
Published: December 23, 2021

ABSTRACT

Aims: Due to population growth and the increase of demand for industrial and agricultural products, many tropical regions of Iran have experienced landscape changes. Satellite imagery and remote sensing (RS) are widely used to map these changes. The present study detects the land use/land cover (LULC) using some pixel-based and object-based classification approaches.
Method: This research was conducted in the Jiroft area, Kerman Province, using Landsat-8 satellite images and some pixel-based and object-based image analyzing methods known as the PBIA and OBIA. To this end, the methodology was carried out in two different phases. At the first one, the LULC maps were extracted using some PBIA techniques for September 2020. These techniques are including as Mahalanobis distance (MD), maximum likelihood (ML), neural network (NN), support vector machine (SVM) as well as unsupervised technique of ISODATA. In the second phase, the LULC was produced using the OBIA approach, encompassing the multi-resolution method and decision tree (DT) technique for segmentation and classification, respectively. To this end, using a hybrid methodology, the high-resolution images of Worldview-2 were firstly segmented. The segmented objects were later combined with the 7-month time series of NDVI, from October (2020) to April (2021), to find the necessary thresholds as the DT inputs. In this regard, the pre-processed Landsat images were trained using ground control points (GCPs), and their performances were finally evaluated.
Findings: Results of the LULC maps demonstrated that the kappa coefficient and overall accuracy for ISODATA, MD, ML, NN, and SVM methods were calculated to be (51%, 66%), (81%, 86%), (88%, 91%), (90%, 93%) and (88% and 92%), respectively. The outcomes of the second phase for mapping the LULC showed that the OBIA achieved a high overall accuracy of about 96%.
Conclusion: Results showed that among the PBIA techniques, the NN and SVM classifiers had slightly superior performance, but regarding both accuracy and execution time, the ML is known to be the best. Although both PBIA and OBIA approaches are highly applicable in mapping LULC, the OBIA significantly outperformed the PBIA classifiers by higher overall accuracy and Kappa statistics.

Keywords: Land cover/Land use; Neural Network; pixel/object-based classifiers.

CITATION LINKS

[1] Sohl T., Sleeter B. 15 Role of ... [2] Akbari H., Rose L.S., Taha H. Analyzing the land cover of an urban environment... [3] Yang L., Xian G., Klaver J.M., Deal B. Urban land-cover change detection ... [4] Gilbertson J.K., Kemp J., Van Niekerk A. Effect ... [5] Rahman M.R., Saha S.K. Multi-resolution ... [6] Karami A., Khoorani A., Noohegar A., Shamsi S.R.F., Moosavi V. Gully ... [7] Rozenstein O., Karnieli A. Comparison of ... [8] Lu D., Weng Q. A survey of image classification methods and... [9] Petropoulos G.P., Kalaitzidis C., Vadrevu K.P. Support vector ... [10] Oyekola M.A., Adewuyi G.K. Unsupervised ... [11] Campbell J.B., Wynne R.H. Introduction ... [12] Fukue K., Shimoda H., Matumae Y., Yamaguchi R., Sakata T. Evaluations of ... [13] Weih R.C., Riggan N.D. Object-based ... [14] Alganci U., Sertel E., Ozdogan M., Ormeci C. Parcel-level ... [15] Myburgh G., Van Niekerk A. Effect of feature dimensionality on ... [16] Zheng B., Myint S.W., Thenkabail... [17] Berhane T.M., Lane C.R., Wu... [18] Coppin P., Lambin E., Jonckheere I., Muys B. Digital... [19] Ghassemian H. A review of remote... [20] Ai J., Gao W., Gao, Z., Shi, R., Zhang... [21] Paola J.D., Schowengerdt R.A. A detailed ... [22] Abburu S., Golla S.B. Satellite image ... [23] Akcay O., Avsar E.O., Inalpulat M., Genc L., Cam A. Assessment of... [24] Benz U.C., Hofmann P., Willhauck G., Lingenfelder I., Heynen M. Multi-resolution...[25] Rwanga S.S., Ndambuki J.M. Accuracy ... [26] Sarkar A. Accuracy assessment ...[27] Behnia N., Zare M., Moosavi V., Khajeddin S.I. Evaluation of a Hierarchical Classification Method and Statistical Comparison with Pixel-Based and Object-Oriented ... [28] Hayatzadeh M., Fathzadeh A., Moosavi V. Improving the Accuracy of Land Use/Cover Maps using an Optimization Technique. ECOPERSIA... [29] Parvizi Y., Heshmati M., Gheituri M. Intelligent approaches to analyze the importance of land use management in soil carbon stock in a semiarid ecosystem, west of Iran. ECOPERSIA...

[DOR: 20.1001.1.23222700.2022.10.1.6.9]

Introduction

In recent years, the population growth and the increase of demand for water and agricultural products, urbanization, and industrialization have changed the land use (LU) and land cover (LC), LULC together, in Iran. As the impacts of LULC changes on climate conditions, carbon dynamics, biodiversity, and hydrology have been recognized, detecting and monitoring such transformations have become increasingly important [1].

LULC refers to the actual surface cover for a given location (e.g., vegetation type and mine structure). Remote sensing (RS) is an effective tool that can be used for producing LULC maps with acceptable accuracy and precision in large areas. RS-based data have a long history of deriving LULC maps, even before the launch of the 1st Landsat platform in 1972. Aerial photography served as a primary source of information on LULC before the availability of satellite imagery [2].

Image classification is the most commonly applied approach in deriving spatially distributed maps of LULC. Many researchers have employed and evaluated various methods to extract LULC maps based on the RS techniques and satellite images. Among these, pixel-based image analysis (PBIA) and object-based image analysis (OBIA) approaches have been widely used. PBIA technique is often used to extract and classify features according to their spectral information. However, the pixels in the overlapping areas will be misclassified due to confusion among the classes. The OBIA approaches use spatial, geometric, and topological information and spectral information in the classification process [3-5].

The PBIA methods can be further divided into unsupervised and supervised classification approaches [6-8]. The unsupervised methods do not require prior knowledge of LULC types before classification, and the interpreter is responsible for assigning a class to each cluster of pixels. The unsupervised classification was developed first through different clustering methods such as K-means and Interactive Self-Organization Data analysis (ISODATA). The supervised approaches use the training samples that are directly taken from the imagery to be classified. They finally group the spectrally similar pixels of a satellite image using various statistical techniques. In addition, decision tree classifiers (known as knowledge-based image classification methods) are a flowchart-like tree structure where an internal node represents a feature (or attribute), the branch represents a decision rule, and each leaf node represents the outcome. [4,5,9-14].

Several studies have employed PBIA and OBIA for LULC and crop type mapping. For example, Weih and Riggan [15] applied the 10m SPOT5 imagery and 1m resolution aerial photography for supervised LULC classifiers. They showed that merging medium, and high spatial resolution imagery significantly enhanced the results of the classification. Alganci *et al.* [16] investigated the accuracy of PBIA and OBIA techniques across varying spatial resolutions to identify crop types. They used Multi-sensor data with spatial resolutions of 2.5m, 5m, and 10m from SPOT-5 and 30m from Landsat-5 TM. Maximum likelihood (ML), spectral angle mapper (SAM), and support vector machines (SVM) were used in their research. They showed that SVM is effective for agricultural classification. Myburgh and Van Niekerk [17] found that SVM is a cost-effective solution for mapping the LULC over large areas. Zheng *et al.* [18] investigated the potential of SVM in discriminating various crop types in a complex cropping system. They applied SVMs to Landsat time-series normalized difference vegetation index (NDVI) data. Results showed that the SVM effectively classified nine major crop types with overall accuracies of >86%.

[DOR: 20.1001.1.23222700.2022.10.1.6.9]

Gilbertson *et al.* [5] evaluated the potential of pan-sharpened Landsat-8 images covering the phenological stages of seven major crops to differentiate them in South Africa. They employed some PBIA/OBIA classifiers like k-nearest neighbor (k-NN), decision trees (DTs), SVM, and random forests (RF). Results showed that the SVM consistently produced superior results while compared to the other classifiers. Berhane *et al.* [19] compared PBIA and OBIA techniques to classify wetlands. They employed different classification approaches such as ISODATA, maximum likelihood (ML), and RF. Results showed that RF and OBIA had the highest accuracy.

Jiroft area is located downstream of Jiroft Dam. Due to its accessible water resources, fertile soil, and humid weather conditions. Therefore, many regions of this tropical county have experienced landscape changes in recent years. This study aims to detect these LULC using both pixel-based and object-based classification approaches. To this end, using some Landsat-8 satellite images and ground control points (GCPs), the PBIA techniques were executed, and the accuracy indices were calculated. Regarding accuracy and execution time, the best PBIA classifier was chosen to be compared with those of the OBIA approach. Next, the material and two-phase methodology of this study and the statistical analysis used for results evaluations are detailed.

Material and Methods

Description of Study Area

The present study was conducted for the Jiroft area, known as the third-order sub-basin of Iran, located south of Kerman Province. It is extending between the latitudes 2914°' 26"N to 2812°' 01"N and the longitudes 57°12' 40"E to 5815°' 27"E. Having an area of 5413 (km^2) and the averaged altitude of 1200 meters (ASL), it covers most of the vast Jiroft plain (Figure 1).

The north-eastern part of this region is mountainous and cold, whereas Jiroft and its surrounding plains have a tropical climate. Rainfall ranges from 200 to 460 mm and

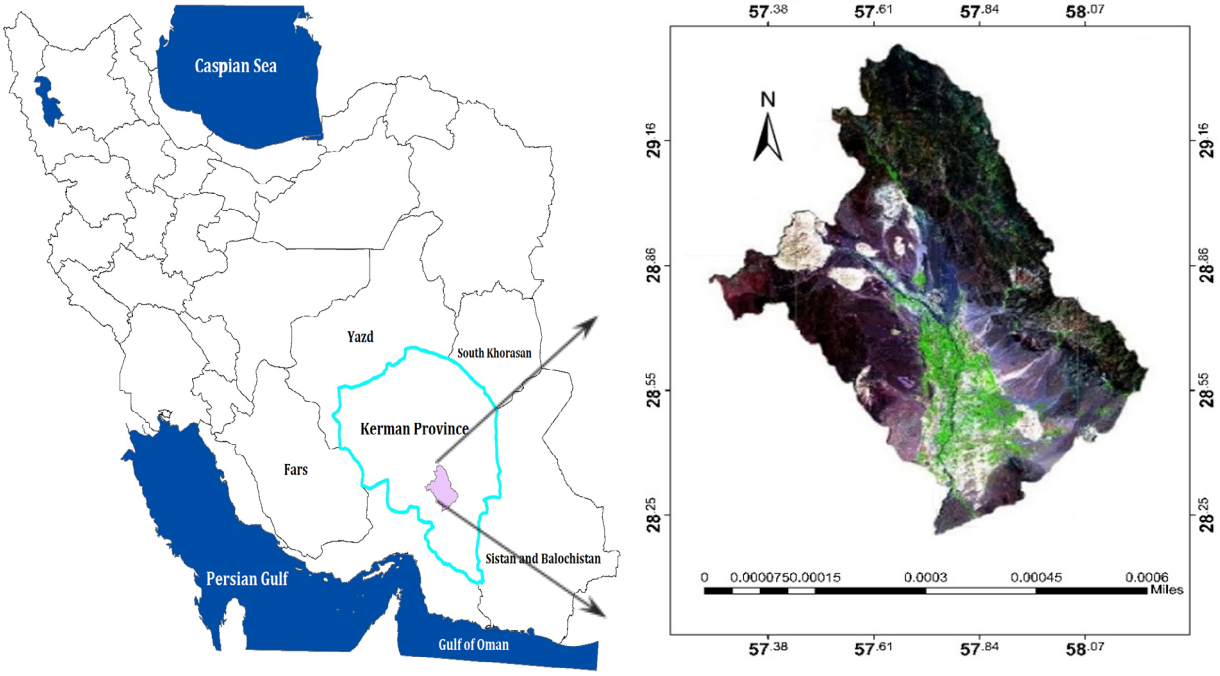

Figure 1) Location of the Jiroft region in Kerman Province, southeast of Iran.

[DOR: 20.1001.1.23222700.2022.10.1.6.9]

occurs mainly from January through April. Jiroft region has a total agricultural area of 14200ha, with a very diverse cropping pattern. Agricultural productivity is the foundation of developing economies in this region. This area produces a wide range of crops (e.g., wheat, barley, Alfalfa, potato, onion, tomato, corn, cereal, and summer crops) and orchards (Citrus, Date palm).

Data Collection

In order to detect the LULC maps at the first phase of this paper, the Landsat-8 imagery data for the Jiroft area was taken from USGS (https://earthexplorer.usgs.gov) including the OLI sensor for September 2020. In the second phase, to detect the LULC maps and compare the OBIA outcomes with the best PBIA classifiers, seven Landsat-8 images for the area were taken. The spectral information of these images for October-December (2020) and January-April (2021) was utilized for LULC classification. The field surveys for collecting the GCPs were carried out in September 2020 and March 2021.

Image Pre-processing

Pre-processing involves geometric and radiometric calibration. Geometric calibration corrects for the angle of view of the satellite sensor, the relief of the terrain, and lens distortions so that images from different sensors at different times can be compared in the same way as maps made using the same projection and scale can be compared. Radiometric calibration is needed because the appearance of the same image varies with the angle of view and illumination conditions.

– ***Radiometric Calibration:*** There are two types of radiometric corrections of satellite images, namely absolute or relative ones. These two methods are usually applied to the images in order to decrease the atmospheric dispersion effects. The first method requires a data entry related to atmospheric properties and sensor calibration. However, in the second one, the dark object subtraction method is used [20].

– ***Images Pan-Sharpening:*** Pan-Sharpening is the process of fusing lower resolution multispectral data with higher resolution panchromatic imagery. This technique often provides a solution to increase the spatial detail of medium resolution of Landsat-8 imagery data [21]. Pan-Sharpening, also known as pan-fusion, has been shown as an effective tool for visual enhancements of imagery [22] and quantitative analyses like land cover mapping [23].

In this research, a Gram-Schmidt pan-sharpening method was used to combine the superior spatial resolution of the 15m panchromatic bands with the spectral information of the lower resolution multispectral bands of Landsat-8 imagery, i.e., 30m optical bands of OLI.

LULC mapping using PBIA and OBIA approaches

In our study, some PBIA classifiers such as MD, ML, NN, and SVM, and OBIA techniques were employed in addition to ISODATA unsupervised technique. A summary of the methodology adopted in the study is illustrated in Figure 2.

As illustrated in Figure 2, at the first phase of the current study, the LULC maps for September 2020 were generated using some PBIA techniques using Landsat-8 satellite images. At the second phase, a high-resolution Worldview-2 image combined with the seven-month time series of Landsat-8 images was used for OBIA evaluation.

Pixel-based image analysis (PBIA)

The PBIA classification relies on the spectral differences between the various phenomena on different spectral bands. So, it does not mean that every phenomenon is distinguishable on any particular band [4, 5]. A brief description of the PBIA classifiers used in our study is presented below.

– ***ISODATA:*** This technique is the most common unsupervised satellite classification

[DOR: 20.1001.1.23222700.2022.10.1.6.9]

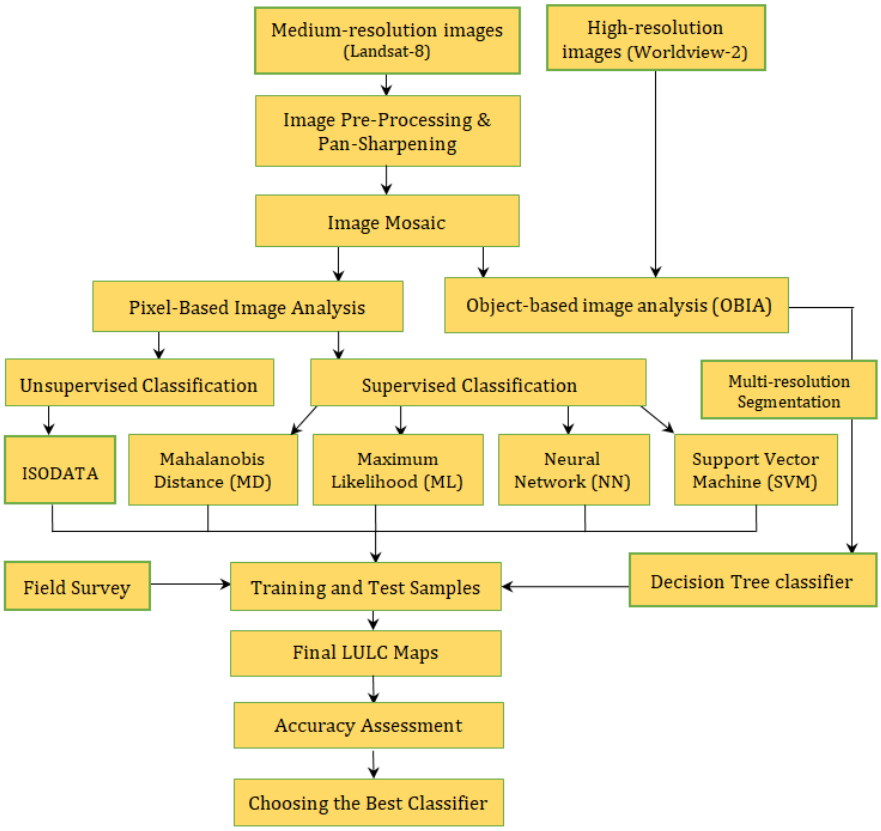

Figure 2) A schematic of the methodology, including PBIA and OBIA, approaches.

method, which creates a predefined number of unlabeled classes. Later meaningful labels are assigned to them. Using the ISODATA method, the software finds the spectral classes or clusters in the multi-band image without the analyst's intervention. Once the clusters are determined, then identifying what the cluster will represent is next, e.g., water, soil, and vegetation [11-14].

– ***Mahalanobis Distance (MD):*** This method is very similar to the minimum distance method. It uses statistics of the covariance matrix for satellite image classification. In the minimum distance approach, the mean spectra of each predefined class are calculated and assigned the pixel to a group that has the least distance to the mean. It is easy to execute and simple to process. However, the minimum distance method considers only the mean value.

– ***Maximum Likelihood (ML):*** ML was built on the assumption that spectral reflectance statistics of each band possess a normal distribution in the n-dimensional image. This method calculates the probability that each pixel in the image space fits best in any candidate classes in the sample space constituted by training sites [16].

– ***Neural Network (NN):*** This technique simulates the human learning process to associate the correct meaningful labels with image pixels. The advantage of NN-based satellite image classification techniques is easy to incorporate supplementary data in the classification process and improves classification accuracy [24].

– ***Support Vector Machine (SVM):*** SVM is a non-parametric statistical classification method. It works on the assumption that there is no information on how to distribute the overall data. The fundamental of the SVM is to map the original data into a higher dimensional feature space by Kernel functions. Its analysis attempts to find a

[DOR: 20.1001.1.23222700.2022.10.1.6.9]

1-dimensional hyperplane (i.e., a line) that separates the cases based on their target categories. It reduces satellite classification costs, increases speed, and improves accuracy. In the classification process, all pixels in the entire object are assigned to the same class, thus removing the problem of spectral variability and mixed pixels [17, 25].

Object-based image analysis (OBIA)

The OBIA typically consists of two processes of segmentation and classification. In this approach, the image information is assessed based on neighboring groups of pixels which spatially have a certain degree of spatial and spectral similarities rather than individual pixels. In the image segmentation stage, an image is split into separate regions or objects depending on the mentioned similarities. Through the classification, similar segmented areas are combined to produce the final LULC maps [6, 7, 10, 15].

– ***Multi-resolution segmentation***

In the current study, we utilized the multi-resolution segmentation algorithm available in eCognition developer commercial software. This algorithm encompasses a bottom-up region-merging process in which a satellite image is subdivided into homogeneous areas according to several defined parameters by the operator. These parameters include band scale, color, shape, weights, smoothness, and compactness. The heterogeneity of the objects becomes more by an increase of the scale parameter. In addition, the shape-color heterogeneities within a determined scale have an impact on segmentation. In this regard, increased heterogeneity in the multi-resolution segmentation is a function of the weighted spectral and shape heterogeneities. Spectral heterogeneity is a standard deviation function depending on the band value and number of pixels in a merged object. The heterogeneity of the shape parameter is also a function of both object smoothness and compactness. The shape criterion can be given a value of up to 0.9. This ratio determines to what degree shape influences the segmentation compared to color. In the same way, the value assigned for compactness gives it a relative weighting against the smoothness. [6, 15, 26-28].

– ***Decision tree (DT) classifier*****:** A DT is a classification method that is also known as a recursive partition of the instance space. It is a common method in data mining that utilizes a series of decisions to segment the data into homogeneous objects. DT model looks like a tree with branches encompassing a lot of splits and nodes. The goal of DT is to determine a set of if-then logical conditions to create a model for estimating the value of a target variable based on several input variables. A tree can be trained by splitting the source set into subsets based on an attribute value test named threshold. This process is repeated recursively for each derived subset. This recursion partitioning is completed when the subset at a node has the same value as the target variable [26, 28].

Accuracy Assessment Indices

The classification methods require inputs from an analyst, known as the training and testing data, and are used for accuracy assessment. The final step in LULC classification is accuracy assessment, which helps us verify our results' accuracy. It is calculated based on the confusion matrix, whose elements are based on the ground control points (GCPs). The GCPs are taken from a field survey and often taken by a GPS receiver.

– ***Overall Accuracy (OA):*** is a measure of accuracy for the whole image across all categories. For calculating OA, a total number of correctly classified pixels (diagonal elements) are divided by the total number of test pixels.

– ***Kappa Coefficient (K):*** Kappa essentially evaluates how well the classification performed compared to just randomly assigning values, i.e., did better than random. The Kappa Coefficient ranges between [0, 1]. A val-

[DOR: 20.1001.1.23222700.2022.10.1.6.9]

ue of 0 demonstrates that the classification is no better than a random classification. A value close to 1 indicates that the classification is significantly better than random.

– ***User's Accuracy (UA):*** The UA is the number of correctly classified pixels in each category divided by the total number of classified pixels in that category. The User's Accuracy is a complement of the Commission Error, User's Accuracy = 1-Commission Error.

– ***Producer's Accuracy (PA):*** PA is the number of correctly classified pixels in each category divided by the total number of classified pixels in that category.

– ***Commission errors (CE):*** Errors of commission occur when a classification procedure assigns pixels to a class that does not belong. In other words, it indicates the land area of a class that does not belong to that class.

– ***Omission error (OE)*** concerns the classified results and refers to the reference sites omitted from the correct class in the classified map. In other words, the OE indicates the land area of a class that belongs to another class [26-30].

Findings

Classification based on PBIA approach

As mentioned previously, at the first phase of the current study, the LULC maps for September 2020 were generated using some PBIA techniques. In this regard, the optical bands of Landsat-8 satellite image were firstly calibrated, and the Gram-Schmidt pan-sharpening method was then employed to combine the superior spatial resolution of the 15m panchromatic bands with the spectral information of the lower resolution multispectral bands of Landsat-8 imagery, i.e., 30m optical bands of OLI.

In order to perform the PBIA techniques and evaluate their results, the GCPs of Jiroft is required. In this regard, before conducting any field survey, a preliminary map of LULC was prepared. So, an unsupervised classification method, i.e., the ISODATA clustering technique, was firstly performed on the image to classify the image into five different classes. The maximum number of iterations and the convergence threshold of ISODATA were set to 15 and 0.95, respectively. A thematic raster layer was finally generated using this technique while running ENVI (Figure 3a). As a result, five classes of the orchard, agriculture, waterbody, rock, and barren lands were identified by ISODATA so that its kappa coefficient and overall accuracy were equaling to 51% and 66%, respectively. Using this initial map, the exact location of GCPs was determined (Figure 3a), and the LULC maps were produced based on these classes (Figure 3b). It should be noted that both residential and arable lands were considered together, and they were classified as a unique class under the name of "barren lands".

During the field survey, a suitable distribution of 1300 GCPs was collected, choosing about 800 points for training and remaining for accuracy assessment. The PBIA techniques including MD, ML, NN, and SVM were firstly trained and then tested using GCPs. The results of these techniques calculated based on the confusion matrix have been presented in Table 1.

According to Table 1, the NN method slightly outperformed the other classifiers by overall accuracy and kappa coefficient of 93% and 90%, respectively. After the NN technique, the SVM method with the OA and K coefficients of 92% and 88% has the best performance, respectively. After that, the SVM and ML classifiers with the overall accuracy and kappa coefficient of (92%, 88%) and (91%, 87%) were respectively, in the second, third-order, and MD performed the worst. Although the NN and SVM were slightly better than ML, their execution time was too-long in our case study. As a result, the ML is the best PBIA classifier and was recom-

[DOR: 20.1001.1.23222700.2022.10.1.6.9]

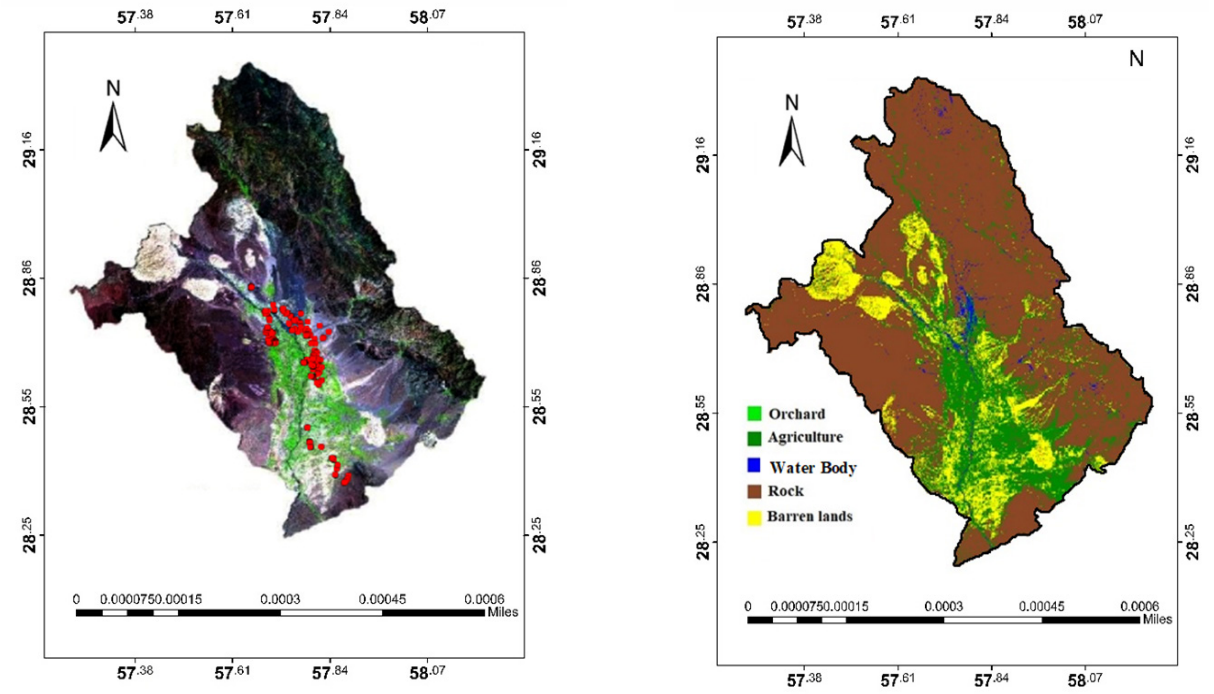

(a) (b)

Figure 3) Location of GCPs, OLI false-color composite: R:6, G: 5, B:4. (a); LULC by ISODATA (b).

mended for accuracy and timely execution in the second phase.

Classification based on OBIA approach

As mentioned before, at the second phase of this study, the OBIA approach and the best PBIA classifier (i.e., ML) were utilized to derive the LULC maps. For this aim, the high-resolution satellite image of World-view-2 with the resolution of about 1m ×1m, covering the whole area of Jiroft county, was first acquired. So, a total number of 11 re-sized scenes were collected (Figure 4a). A multi-resolution segmentation algorithm then carried out the segmentation proce-dure. This procedure was generally man-aged by assigning an appropriate value of three main factors: scale, shape, and com-pactness. So, the best scale, shape, and com-pactness parameters for orchard and agri-cultural areas were assessed as 170, 0.6, and 0.1, respectively.

The seven-month time series of Land-sat-8 images for 2020 (October-December) and 2021 (January-April) were secondly pre-processed, and the medium-resolution time series of NDVI was later generated us-ing the pan-sharpened imagery. Figure 4a illustrates the location of 11 high-resolution scenes and the role of the scale parameter in finding the best segmentation parameters. As shown in Figures 4b and 4c, the best value of the scale was assessed as 170, while the other segmentation parameters remained constant. With this scale, the objects are cre-ated as similar to the crop fields. For the rest of the region with broad rangelands, bar-ren lands, residential areas, mountains, and rocks, called non-agricultural areas, the best scale, shape, and compactness parameters were assessed as 1000, 0.6, and 0.1, respec-tively. The accuracy of segmentation was fi-nally investigated using trail-error based on the visual evaluation.

Having segmented the images, the DT was afterward implemented to classify the LULC. In order to differentiate wide ranges of LULCs, some NDVI thresholds were chosen for both agricultural and non-agricultural

[DOR: 20.1001.1.23222700.2022.10.1.6.9]

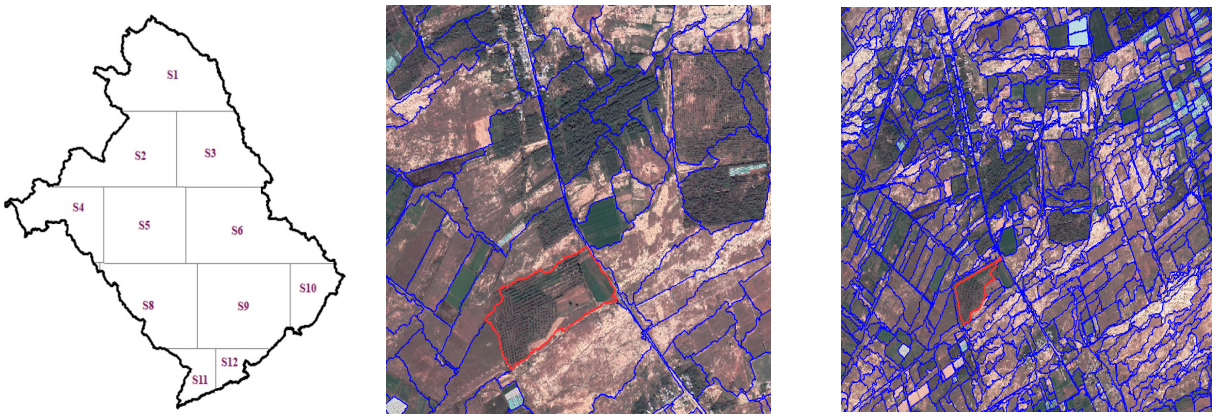

(a) (b) (c)

Scale=200, Shape=0.6,Compact=0.1 Scale=170, Shape=0.6, Compact=0.1

Figure 4) Illustration of 11 high-resolution and resized scenes for OBIA approach (a), partial segmentation output of multi-resolution approach at the scale of 200(b) and 170 (c).

Table 1) The accuracy indices were calculated from the confusion matrix for Jiroft LULC classification.

Accuracy Indices								
Classifiers		Class	OA(%)	K(%)	UA(%)	PA(%)	CE(%)	OE (%)
	MD	Orchard	86	81	98.2	81.7	1.8	18.3
		Agriculture			42.3	82.5	56.8	17.5
		Water Body			100.0	99.4	0.0	0.6
		Rock			86.1	90.2	13.9	9.8
		Barren lands			86.4	81.8	13.6	18.2
	ML	Orchard	91	87	97.8	87.8	2.2	12.2
		Agriculture			53.1	88.1	46.9	11.9
		Water Body			100.0	99.6	0.0	0.4
		Rock			90.3	99.4	9.7	5.6
		Barren lands			92.5	86.7	7.5	13.3
	NN	Orchard	93	90	94.7	89.2	5.3	10.8
		Agriculture			50.8	66.0	49.2	34.0
		Water Body			100.0	99.7	0.0	0.3
		Rock			90.3	97.5	7.7	2.5
		Barren lands			96.6	90.1	3.4	9.9
	SVM	Orchard	92	88	92.8	94.0	7.2	6.0
		Agriculture			61.2	55.8	38.9	44.2
		Water Body			100.0	99.4	0.0	0.6
		Rock			93.9	90.6	6.1	9.4
		Barren lands			88.6	92.7	11.4	7.3

[DOR: 20.1001.1.23222700.2022.10.1.6.9]

areas. The time series of NDVI for the years 2020 (October-December) and 2021 (January-April) were generated to set up the temporal characteristic of each segmented object. The NDVI time series were subsequently combined with cultivation data to extract the thresholds for the DT technique.

To design and evaluate the DT model, among 700 GCPs, collected from the field surveys in September 2020 and March 2021, about 70% and 30% were chosen as the training and testing samples, respectively. To train DTs, the average and standard deviation of NDVI for each segmented object were calculated, and the NDVI thresholds for different classes of LULC were finally extracted. These thresholds are essential for writing the if-then conditional statements (rules). The rules of the 9th scene of the case study are stated as below (Figure 5).

– Through the first rule, the orchard, agricultural land, and rangeland classes were separated using a 7-month average of NDVI by selecting 0.1 as the threshold. So the NDVI ≤0.1 was assigned to the "barren lands" class.

– Next, the threshold of 0.3 and 0.27 for the 7-month average of NDVI and the NDVI value for October 2020 were respectively chosen to differentiate orchards from agricultural areas and rangeland classes.

– After separating the land-uses as mentioned above, rangelands and late-season varieties of agricultural lands were separated using the NDVI threshold of 0.32 for December 2020.

Having prepared the DT model for the whole study area, the confusion matrix and relevant accuracy assessment indices evaluated its performance. Besides employing the OBIA at the second phase of this study, the best classifier from PBIA techniques, i.e., ML was also trained and then tested to compare its LULC map with ones derived from OBIA. Figure 6 illustrates the LULC maps produced by OBIA and PBIA approaches.

The accuracy indices demonstrated the overall accuracy (OA) and Kappa coefficient equal to (96%, 92%) and (77%, 70%) for OBIA and PBIA, respectively. In the OBIA approach, it is worth mentioning that the highest values of producer's accuracy (PA=95%) and user's accuracy (UA=98%) belong to the barren land class. The producer's and user's accuracy for agricultural lands are 70% and 88.4%, respectively. This means that 70% of the agricultural lands are correctly detected, and 88.4% of the regions that were classified as agricultural lands are actually inside this class. For this class of LULC, the PA and UA values in the PBIA approach were 87.6% and 57%, respectively. Comparisons of the accuracy indices also indicated that the PBIA was less accurate than OBIA for detecting the rangeland classes.

Discussion

At the first phase of this study, the LULC maps for September of 2020 were produced using supervised PBIA classifiers like MD, ML, NN, and SVM and the unsupervised technique of ISODATA. In this regard, five orchard classes, agriculture, waterbody, rock, and barren lands, were chosen. Regarding the diversity of crops and variability of their vegetation density, the agricultural lands had the least values of producer's and user's accuracy, equaling an average of 73% and 52% for all classifiers, respectively. The results of the first phase also indicated that the NN slightly outperformed the SVM and ML classifiers. However, for both accuracy and execution time, the ML is known as the best PBIA classifier and was recommended for the second phase.

The LULC maps were produced using both PBIA (ML classifier) and OBIA approaches in the second phase. In this regard, 1m resolution Worldview-2 imagery was utilized to create the segmented objects more precisely. These objects were later combined with medium-resolution of NDVI (generated from

[DOR: 20.1001.1.23222700.2022.10.1.6.9]

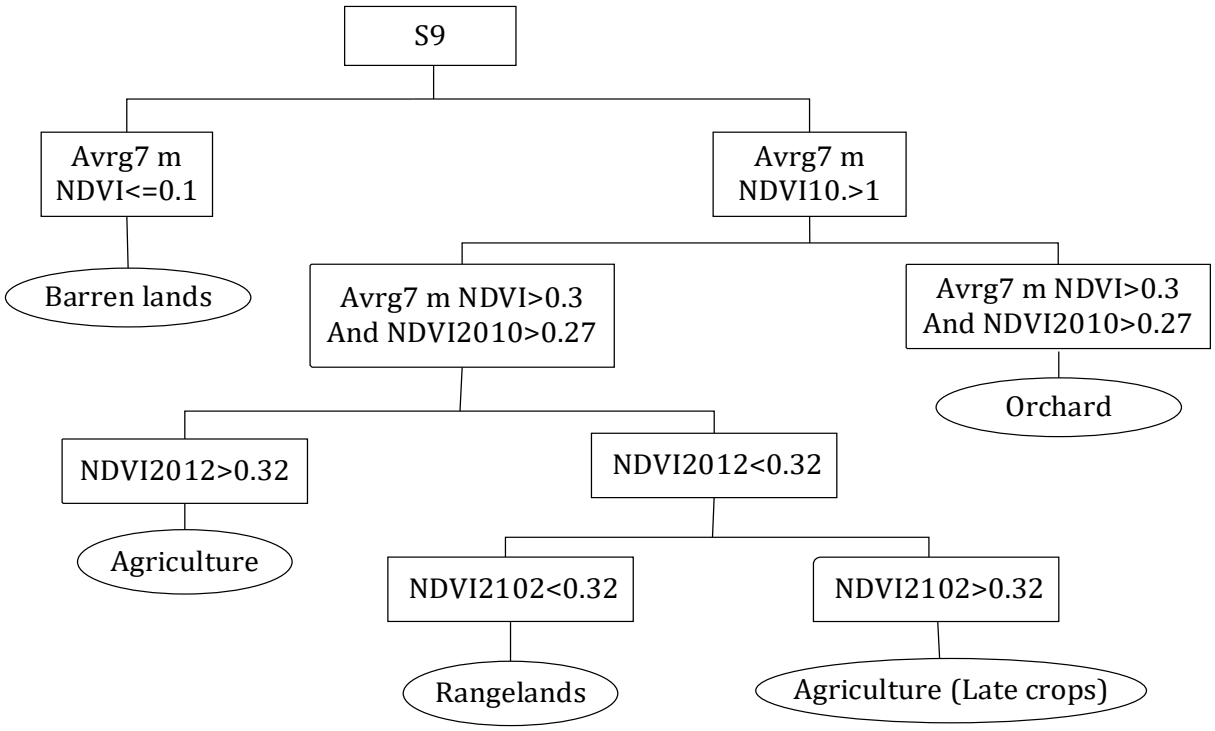

Figure 5) Schematic of the designed DT for the 9th scene of the Jiroft area.

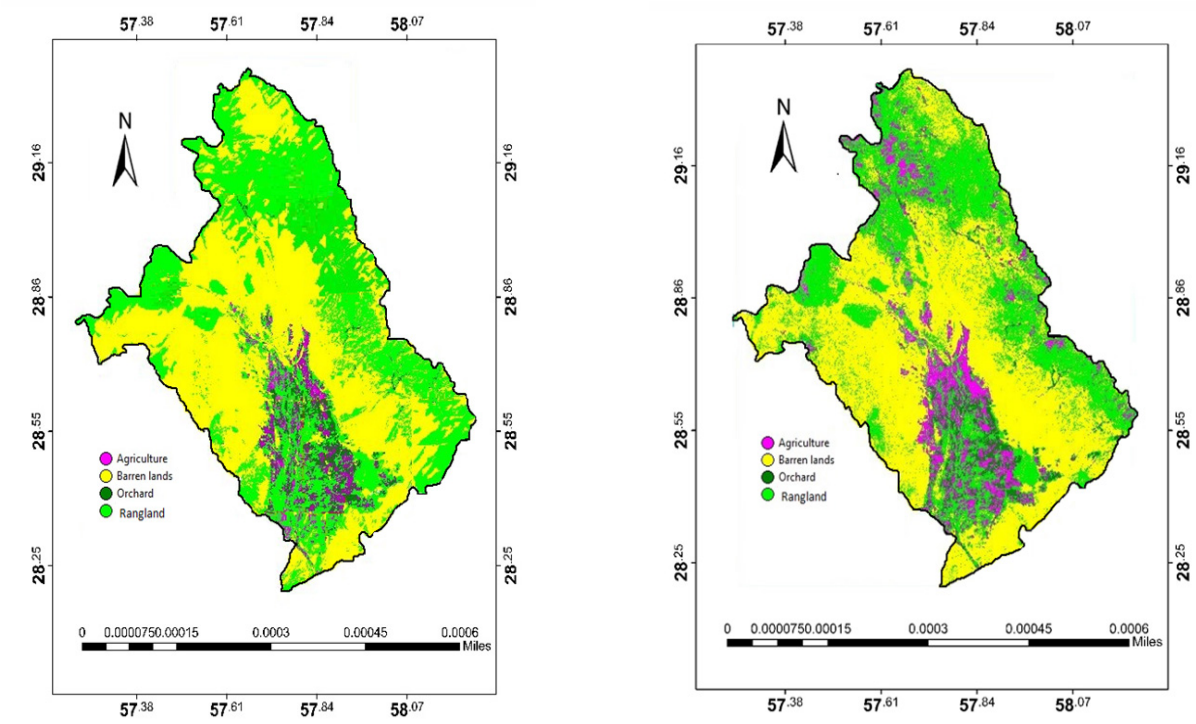

(a) (b)

Figure 6) LULC map produced by two approaches of OBIA (a) and PBIA (b) .

Landsat-8 images) to discover the necessary thresholds of the DT technique.

Since the water body class was not considerable in extent and not separable in NDVI

[DOR: 20.1001.1.23222700.2022.10.1.6.9]

values, this class was eliminated during the second phase. Moreover, conducting the field surveys and monitoring the spectral-temporal behavior of the 7-month time series of NDVI proved that the rangelands covered many mountainous areas and rocky lands. Therefore the orchard, agriculture, barren land, and rangeland were chosen as the main classes of this phase. Based on the confusion matrix resulting from the second phase, the OBIA significantly outperformed the PBIA approach by an overall accuracy of 96% and the Kappa coefficient of 92%. Similar to the first phase, the agricultural areas detected by the OBIA approach have the least values of accuracy indices while compared to other classes. The superiority of OBIA may be attributed to several reasons. Other phenomena like shape, color, and scale are involved in the OBIA approach, apart from spectral properties. The application of high-resolution images inside the hybrid method could also enhance the accuracy of the OBIA approach in our case study.

Conclusion

Accurate and up-to-date LULC maps are essential for yield forecasting and agricultural planning. This issue becomes more critical for regions like Jiroft, which are dominated by massive diversity of crops, palm dates, citrus, and rangelands. Moreover, classifying satellite images to extract accurate and reliable LULC information is still challenging because of image type, landscape complexity, and image classification techniques. The outcomes showed that to both accuracy indices and execution time, the ML outperformed the other PBIA classifiers. The MD was known to be the worst classifier in our case study. By applying the hybrid approach in the second phase, we were able to take advantage of the high-resolution images (Worldview-2) in the segmentation procedure and combined them with medium-resolution images of NDVI, derived from Landsat-8 image, for LULC classification. Regarding the diversity of crops, variability of their vegetation density, changeable crop calendar in the Jiroft region, the agricultural land class had the least accuracy in both PBIA, and OBIA approaches.

Acknowledgments

The authors would like to thank the Graduate University of Advanced Technology, who provided the facilities to do this study.

Ethical permissions: The authors ensure that they have written entirely original works, and if the authors have used the work and words of others, they have been appropriately cited or quoted.

Conflicts of Interests: The corresponding author has no conflict of interest.

Authors' Contribution: Eslami A. (First author), Original researcher (30%), Anvari S. (Second author), Original researcher (45%), Karimi N. (Third author), Methodologist/ Discussion author (20%), Mohammadi S. (fourth author), Assistant (5%).

References

1. Sohl T., Sleeter B. 15 Role of Remote Sensing for Land-Use and Land-Cover Change Modeling. Remote Sens. 2012;1(1): 225-240.
2. Akbari H., Rose L.S., Taha H. Analyzing the land cover of an urban environment using high-resolution orthophotos. Landscape Urban Plan. 2003; 63(1): 1-4.
3. Yang L., Xian G., Klaver J.M., Deal B. Urban land-cover change detection through sub-pixel imperviousness mapping using remotely sensed data. Photogramm. Eng. Remote Sens. 2003; 69(9):1003-1010.
4. Gilbertson J.K., Kemp J., Van Niekerk A. Effect of pan-sharpening multi-temporal Landsat 8 imagery for crop type differentiation using different classification techniques. Comput. Electron. Agr. 2017; 134(2):151-159.
5. Rahman M.R., Saha S.K. Multi-resolution segmentation for object-based classification and accuracy assessment of land use/land cover classification using remotely sensed data. J. Indian Soc. Remote 2008; 36(2):189-201.
6. Karami A., Khoorani A., Noohegar A., Shamsi

[DOR: 20.1001.1.23222700.2022.10.1.6.9]

S.R.F., Moosavi V. Gully erosion mapping using object-based and pixel-based image classification methods. Environ. Eng. Geosci. 2015; 21(2): 101-110.
7. Rozenstein O., Karnieli A. Comparison of methods for land-use classification incorporating remote sensing and GIS inputs. Appl. Geogr. 2011; 31(2): 533-544.
8. Lu D., Weng Q. A survey of image classification methods and techniques for improving classification performance. Int. J. Remote Sens. 2007; 28(5): 823–870.
9. Petropoulos G.P., Kalaitzidis C., Vadrevu K.P. Support vector machines and object-based classification for obtaining land-use/cover cartography from Hyperion hyperspectral imagery. Comput. Geosci. 2012; 41(12):99-107.
10. Oyekola M.A., Adewuyi G.K. Unsupervised classification in land cover types using remote sensing and GIS techniques. Int. J. Sci. Eng. Invest. 2018; 7(72): 11-18.
11. Campbell J.B., Wynne R.H. Introduction to remote sensing. Guilford Press; 2011 Jun 21:667p.
12. Fukue K., Shimoda H., Matumae Y., Yamaguchi R., Sakata T. Evaluations of unsupervised methods for land-cover/use classifications of Landsat TM data. Geocarto. Int. 1988; 3(2): 37-44.
13. Weih R.C., Riggan N.D. Object-based classification vs. pixel-based classification: Comparative importance of multi-resolution imagery. Remote Sen. Spat. Inf. Sci. 2010; 38(4):1-6.
14. Alganci U., Sertel E., Ozdogan M., Ormeci C. Parcel-level identification of crop types using different classification algorithms and multi-resolution imagery in Southeastern Turkey. Photogram Eng. Remote Sens. 2013; 79(11): 1053-1065.
15. Myburgh G., Van Niekerk A. Effect of feature dimensionality on object-based land cover classification: A comparison of three classifiers. S. Afr. J. Geol. 2013; 2(1): 13-27.
16. Zheng B., Myint S.W., Thenkabail P.S., Aggarwal R.M. A support vector machine to identify irrigated crop types using time-series Landsat NDVI data. Int. J. Appl. Earth. Obs. 2015; 34(1):103-112.
17. Berhane T.M., Lane C.R., Wu Q., Anenkhonov O.A., Chepinoga V.V., Autrey B.C. Comparing pixel-and object-based approaches in effectively classifying wetland-dominated landscapes. Remote Sens. Basel. 2018; 10(1): 1-28.
18. Coppin P., Lambin E., Jonckheere I., Muys B. Digital change detection methods in natural ecosystem monitoring: A review. Ser. Remote Sens. 2002;25(9):1565-1596.
19. Ghassemian H. A review of remote sensing image fusion methods. Inform. Fusion. 2016; 32(1):75-89.
20. Ai J., Gao W., Gao, Z., Shi, R., Zhang C., Liu C. Integrating pan-sharpening and classifier ensemble techniques to map an invasive plant in an estuarine wetland using Landsat 8 imagery. J. Appl. Remote Sens. 2016; 10(2):1-17.
21. Paola J.D., Schowengerdt R.A. A detailed comparison of backpropagation neural network and maximum-likelihood classifiers for urban land use classification. IEEE T. Geosci. Remote 1995; 33(4):981-996.
22. Abburu S., Golla S.B. Satellite image classification methods and techniques: A review. Int. J. Comput. Appl. 2015; 119(8):20-25.
23. Akcay O., Avsar E.O., Inalpulat M., Genc L., Cam A. Assessment of segmentation parameters for object-based land cover classification using color-infrared imagery. ISPRS. Int. Geo-Inf. 2018 Nov; 7(11):1-26.
24. Benz U.C., Hofmann P., Willhauck G., Lingenfelder I., Heynen M. Multi-resolution, object-oriented fuzzy analysis of remote sensing data for GIS-ready information. ISPRS J. Photogrammetry 2004; 58(3-4):239–258.
25. Rwanga S.S., Ndambuki J.M. Accuracy assessment of land use/land cover classification using remote sensing and GIS. Int. J. Geosci. 2017; 8(4): 1-13.
26. Sarkar A. Accuracy assessment and analysis of land use land cover change using geoinformatics technique in Raniganj coalfield area, India. Int. J. Env. Sci. Nat. Res. 2018; 11(1):25-34
27. Behnia N., Zare M., Moosavi V., Khajeddin S.I. Evaluation of a Hierarchical Classification Method and Statistical Comparison with Pixel-Based and Object-Oriented Approaches. ECOPERSIA 2020; 8(4):209-219.
28. Hayatzadeh M., Fathzadeh A., Moosavi V. Improving the Accuracy of Land Use/Cover Maps using an Optimization Technique. ECOPERSIA 2019; 7(4):183-193.
29. Parvizi Y., Heshmati M., Gheituri M. Intelligent approaches to analyze the importance of land use management in soil carbon stock in a semiarid ecosystem, west of Iran. ECOPERSIA 2017; 5(1):1699-1709.

[DOR: 20.1001.1.23222700.2022.10.1.6.9]